J. Fluid Mech. (1995), *vol.* 300, *pp.* 287–309

Nonlinear compressible magnetoconvection. Part 3. Travelling waves in a horizontal field

By D. P. BROWNJOHN, N. E. HURLBURT†, M. R. E. PROCTOR AND N. O. WEISS

Department of Applied Mathematics and Theoretical Physics, University of Cambridge, Silver Street, Cambridge CB3 9EW, UK

(Received 20 June 1994 and in revised form 15 May 1995)

We present results of numerical experiments on two-dimensional compressible convection in a polytropic layer with an imposed horizontal magnetic field. Our aim is to determine how far this geometry favours the occurrence of travelling waves. We therefore delineate the region of parameter space where travelling waves are stable, explore the ways in which they lose stability and investigate the physical mechanisms that are involved. In the magnetically dominated regime (with the plasma beta, $\hat{\beta} = 8$), convection sets in at an oscillatory bifurcation and travelling waves are preferred to standing waves. Standing waves are stable in the strong-field regime ($\hat{\beta} = 32$) but travelling waves are again preferred in the intermediate region ($\hat{\beta} = 128$), as suggested by weakly nonlinear Boussinesq results. In the weak-field regime ($\hat{\beta} \geqslant 512$) the steady nonlinear solution undergoes symmetry-breaking bifurcations that lead to travelling waves and to pulsating waves as the Rayleigh number, $\hat{R}$, is increased. The numerical experiments are interpreted by reference to the bifurcation structure in the $(\hat{\beta}, \hat{R})$-plane, which is dominated by the presence of two multiple (Takens–Bogdanov) bifurcations. Physically, the travelling waves correspond to slow magnetoacoustic modes, which travel along the magnetic field and are convectively excited. We conclude that they are indeed more prevalent when the field is horizontal than when it is vertical.

1. Introduction

Sunspots and starspots provide the astrophysical motivation for studying convection in a strong magnetic field. In Part 1 (Hurlburt *et al.* 1989) and Part 2 (Proctor *et al.* 1994) of this series we described time-dependent behaviour when the imposed field is vertical, and further effects of stratification were explored by Weiss *et al.* (1990). That configuration relates to the dark central umbra of a sunspot but the field lines fan out in the penumbra, becoming almost horizontal at its outer edge. The bright and dark filaments in the penumbra are associated with a complicated magnetic structure (Thomas & Weiss 1992) but there is as yet no adequate model of penumbral convection. It seems clear, however, that the transition from a pore (corresponding to an isolated umbra) to a spot (with a filamentary penumbra) is associated with the sudden development of filamentary convection (Rucklidge, Schmidt & Weiss 1995). This can be modelled as a three-dimensional instability of an axisymmetric

† Permanent address: Lockheed Palo Alto Research Laboratories, Palo Alto, CA 94304, USA.

poloidal circulation. Indeed, penumbral waves, which run outwards as concentric arcs enclosing a large fraction of a spot (Lites 1992), provide evidence of a form of convectively excited motion that is effectively axisymmetric. So we first need to explore the effects of different field geometries on convection. In an inclined field convection may take the form of travelling waves with the velocity confined to vertical planes containing the magnetic field (Matthews *et al.* 1992; Hurlburt, Matthews & Proctor 1995) rather than rolls with axes lying in such planes (Chandrasekhar 1961). With a horizontal field convection is unimpeded if it takes place in rolls aligned with the magnetic field. This configuration would be relevant if sunspots had shallow penumbrae – but observations confirm that penumbrae must be deep. Then simple models show that convection has to transport energy inwards across the field from the external plasma. Thus it is appropriate to investigate the idealized problem of two-dimensional convection in rolls whose axes are perpendicular to the magnetic field. We regard this study as a necessary preliminary to more ambitious models of penumbral structure, which is intrinsically three-dimensional.

There is another, fluid dynamical motivation for studying this problem. Magnetoconvection is an important example of 'double convection', where there are competing stabilizing and destabilizing mechanisms (in this case, the magnetic field and the superadiabatic temperature gradient) with different characteristic diffusion times. Such competition often leads to oscillatory behaviour. With periodic lateral boundary conditions, a Hopf bifurcation gives rise to travelling and standing wave solutions, and nonlinear processes determine which of these is preferred. It is natural to seek a physical argument as well. In the presence of a magnetic field a convecting layer acts as a waveguide for slow magnetoacoustic waves which travel along the field (cf. Part 1). Intuitively, one might expect travelling waves to be preferred if the field is horizontal, while standing waves should be more likely if the field is vertical. Numerical experiments can determine whether this naive argument is valid. In such problems there is a competition between physical processes and the constraints imposed by bifurcation theory. The computations reveal a rich underlying bifurcation structure, involving interactions between travelling waves, standing waves and other types of oscillation, such as pulsating waves, that are permitted by the symmetries (Proctor & Weiss 1993; Matthews *et al.* 1993). In fact, this problem provides a fine demonstration of the way in which such a bifurcation structure can be used to interpret the numerical results.

Boussinesq magnetoconvection in a horizontal field was first investigated by Arter (1983) but his mirror-symmetric lateral boundary conditions excluded travelling waves. In the regime of interest, convection sets at a Hopf bifurcation, giving rise to a branch of standing wave solutions, at a Rayleigh number $R = R^{(o)}$. This oscillatory branch terminates in a heteroclinic bifurcation, on an unstable section of the branch of steady solutions emerging from a pitchfork bifurcation at $R = R^{(e)} > R^{(o)}$. Although there are (unstable) weakly nonlinear steady solutions for R slightly greater than $R^{(e)}$, the steady branch has two turning points and stable steady solutions first appear at $R = R_{\min}$, where $R^{(o)} < R_{\min} < R^{(e)}$. This bifurcation structure is similar to that found when the field is vertical (Proctor & Weiss 1982).

Knobloch (1986) studied the effect of introducing periodic lateral boundary conditions, which allow travelling waves as well as standing waves in the the same parameter regime. He found that travelling waves are stable (and standing waves unstable) in the immediate neighbourhood of the double Takens–Bogdanov bifurcation (where $R^{(o)} = R^{(e)}$). In the analogous situation with a vertical field, standing waves tend to be preferred (Dangelmayr & Knobloch 1986). It is not clear how far these

results extend into the nonlinear regime if there are turning points on the steady branch or if the Hopf and pitchfork bifurcations are no longer close. With a vertical field, a systematic survey showed that either travelling waves or standing waves may be preferred in the Boussinesq limit, depending on the parameters, and that there was no straightforward way of predicting the result (Matthews & Rucklidge 1993). Numerical experiments on compressible magnetoconvection (Hurlburt & Toomre 1988; Parts 1 and 2) reveal a general preference for standing waves, except in the regime where the ratio of gas pressure to magnetic pressure (the plasma beta, $\hat{\beta}$) is small, as well as a great variety of periodic, quasi-periodic and chaotic oscillations.

This paper differs in three ways from Arter's study of convection in a horizontal field. First, the fluid layer is stratified: although there is no great variation in density, the up-down symmetry of the Boussinesq problem is absent, symmetry properties of solutions are changed and the bifurcation structure is affected (Proctor & Weiss 1993; Matthews *et al.* 1993). Second, effects of compressibility are included and become important when $\hat{\beta}$ approaches unity. Third, and most important, we adopt periodic lateral boundary conditions, which allow a range of symmetry-breaking bifurcations; solutions found with fixed lateral boundaries may therefore prove unstable. A similar configuration, with different boundary conditions at the top and bottom of the layer, has been studied by Lantz & Sudan (1995; Lantz 1995) in the anelastic approximation.

Our numerical experiments yield examples of several different types of nonlinear solution. After a pitchfork bifurcation convection sets in as a steady solution (SS), which is stationary in the frame with zero net momentum, but a Hopf bifurcation gives rise to periodic standing waves (SW), i.e. stationary oscillations with reversals of the flow, and to travelling waves (TW), which are stationary in a uniformly moving frame. Secondary bifurcations lead to modulated waves (MW), which are periodic in a uniformly moving frame, and to pulsating waves (PW), which are periodic and have a symmetry such that advancing half a period in time is equivalent to reflection about a vertical plane. The interactions between these solutions give rise to complicated patterns of behaviour, which cannot be understood until the underlying bifurcation structure has been established. Our aim, therefore, is to infer the bifurcation structure from the numerical results. In describing them, we shall concentrate on qualitative features but it is also essential to list the quantitative details that justify our assertions.

We have carried out a systematic numerical investigation of nonlinear behaviour over the range $1500 \leqslant \hat{R} \leqslant 128000$, where $\hat{R}$ is the Rayleigh number, defined (like other dimensionless quantities) in Parts 1 and 2, for $\hat{\beta} \geqslant 8$ and we find four different regimes depending on the strength of the imposed magnetic field. The stability boundary, beyond which convection is suppressed by the magnetic field, lies close to $\hat{\beta} = 8$ when $\hat{R}$ is large. Near this boundary is a magnetically dominated regime, where fluctuations in magnetic pressure are important: for $\hat{\beta} = 8$ travelling waves are preferred, as in a vertical field. With strong fields ($\hat{\beta} = 32$) there is a transition from standing waves via modulated waves to travelling waves as $\hat{R}$ is increased; some of these results have been reproduced in reviews (Weiss 1991; Proctor 1992) and presented as a video. In the intermediate-field regime ($512 \gtrsim \hat{\beta} \gtrsim 128$) behaviour is essentially Boussinesq and travelling waves are preferred until streaming instabilities lead to pulsating waves at high $\hat{R}$. Finally, in the weak-field limit ($\hat{\beta} \gtrsim 8192$) the Lorentz force is insignificant and hydrodynamic behaviour is only affected by compressibility at high Rayleigh numbers.

The paper is organized as follows. In the next section we define the model configuration and investigate its linear stability. In §3 we explore weakly nonlinear

behaviour and describe the competition between standing waves and travelling waves in the oscillatory regime. Then, in §4, we study interactions between travelling waves and steady convection in the intermediate- and weak-field regimes, and establish the relevant bifurcation structures. Transitions to pulsating waves, from steady convection and from travelling waves, are briefly discussed in §5; this allows us to construct the final bifurcation diagram, which is dominated by a pair of codimension-two (Takens–Bogdanov) bifurcations. In the last section we draw conclusions from these results and relate them to behaviour in other doubly-convective systems.

2. The model problem

We shall investigate fully compressible two-dimensional magnetoconvection in a perfect monatomic gas. The configuration differs from that described in Parts 1 and 2 only in that the imposed magnetic field is horizontal and not vertical, so there is no need to repeat the details here. The dimensionless temperature T, velocity $\boldsymbol{u}$ and magnetic field $\boldsymbol{B}$ satisfy the partial differential equations (2.1)–(2.4) of Part 2 in the region $\{0 \leqslant x \leqslant \lambda;\ z_0 < z < z_0 + 1\}$, where symbols are defined in Parts 1 and 2. The layer is heated uniformly from below, so that $T(x, z_0) = z_0$, $T(x, z_0 + 1) = z_0 + 1$, and the velocity satisfies the usual stress-free boundary conditions, so that $u_z = \partial u_x/\partial z = 0$ at $z = z_0, z_0 + 1$. The vertical component of the magnetic field vanishes at the upper and lower boundaries and the total magnetic flux remains constant, so that the horizontal component of the electric field $\boldsymbol{E} = \zeta_0 \bar{K} \nabla \times \boldsymbol{B} - \boldsymbol{u} \times \boldsymbol{B}$ vanishes at the top and bottom of the layer. This is equivalent to assuming that the boundaries are perfectly conducting. It follows therefore that

$$B_z = \frac{\partial B_x}{\partial z} = 0 \quad \text{at } z = z_0, z_0 + 1. \tag{2.1}$$

We assume lateral periodicity: all quantities are periodic in x, with period λ, so that $T(0, z) = T(\lambda, z)$ etc.

The static reference atmosphere is a polytrope with $T = z$ and a density $\rho = (z/z_0)^m$; we take $z_0 = \frac{1}{6}$ and a polytropic index $m = \frac{1}{4}$, so that the atmosphere is only weakly stratified. The ratios of the viscous and magnetic diffusivities to the thermal diffusivity are set so that $\sigma = \hat{\zeta} = 0.1$ (where circumflexes denote values at the middle of the layer). Then the state of the configuration is defined by two parameters: the Rayleigh number $\hat{R}$, and either the plasma beta $\hat{\beta}$ or the Chandrasekhar number $Q = 128\hat{R}/9\hat{\beta}$.

We have studied the stability of the static atmosphere with the aid of a program developed by Cattaneo (1984). Since the layer is only weakly stratified the values of $\hat{R}^{(e)}$ and $\hat{R}^{(o)}$ are close to the corresponding values $R^{(e)}$ and $R^{(o)}$ for a Boussinesq fluid. For square rolls with an aspect ratio $\lambda = 2$, the case with which we shall be most concerned, $R^{(e)}$ or $R^{(o)}$ are the same for horizontal and vertical fields; so linear theory yields results that are similar to those quoted in Parts 1 and 2. Convection sets in at a stationary (pitchfork) bifurcation when the field is weak and there is a Takens–Bogdanov bifurcation ($\hat{R}^{(e)} = \hat{R}^{(o)}$) at $\hat{\beta} = 495$, with $\hat{R} = 1877$ and $Q = 54$. For $\hat{\beta} < 495$ instability appears at an oscillatory (Hopf) bifurcation. Table 1 lists $\hat{R}^{(o)}$ and $\hat{R}^{(e)}$ for values of $\hat{\beta}$ and Q that are relevant later in this paper. We have also compared the behaviour of $\hat{R}^{(o)}$ as a function of Q for three different aspect ratios, $\lambda = 1$, 2 and 4. For $Q < 1000$ the values of $\hat{R}^{(o)}$ for $\lambda = 2, 4$ are very close, with

$\hat{\beta}$	$\hat{R}^{(o)}$	Q	$\hat{\beta}$	$\hat{R}^{(e)}$	Q
8	10900	19370	512	1809	50.2
16	2784	2475	1024	1175	16.3
32	2210	982	2048	998	6.9
64	2016	448	4096	929	3.2
128	1934	215	8192	871	1.5
256	1895	105	∞	869	0

TABLE 1. Linear theory: bifurcation values ($\lambda = 2$).

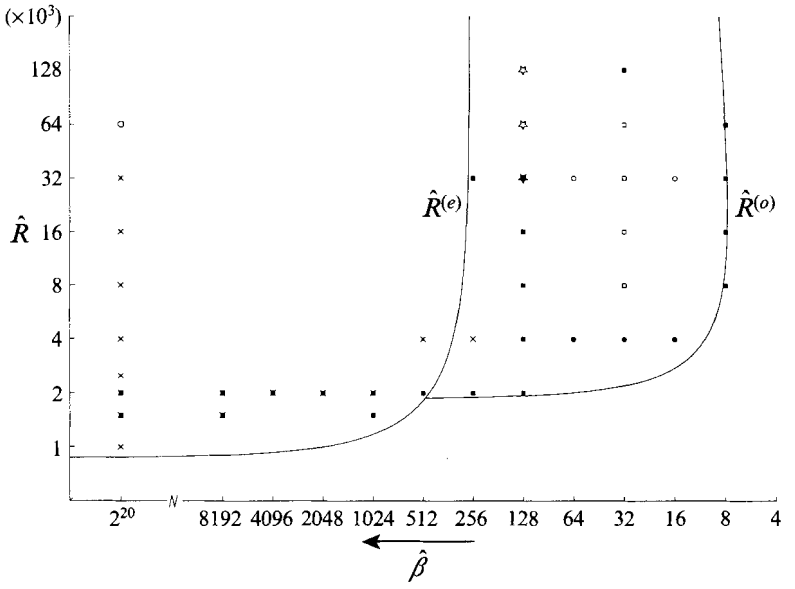

FIGURE 1. Location of computed nonlinear solutions in the $(\hat{\beta}, \hat{R})$-plane for $\lambda = 2$. Travelling waves (TW) are indicated by filled squares, standing waves (SW) by filled circles, pulsating waves (PW) by stars and steady solutions (SS) by crosses. Hollow squares and hollow circles denote modulated waves (MW) and quasi-periodic solutions, respectively. Where crosses (stars) are superposed on squares SS (PW) and TW are both stable. The lines of stationary and oscillatory bifurcations, at $\hat{R} = \hat{R}^{(e)}$, $\hat{R}^{(o)}$, are also marked.

that for $\lambda = 2$ very slightly lower. For $Q > 1000$ the strong field favours flatter cells and $\hat{R}^{(o)}$ is less for $\lambda = 4$. The bifurcation values for $\lambda = 1$ always lie above those for $\lambda = 2$, in contrast to behaviour in a strong vertical field, where narrower cells are preferred.

In what follows, we present nonlinear results obtained numerically, using the two-step Lax–Wendroff scheme described in Part 1; the code is a modification of that used by Hurlburt & Toomre (1988). For nearly all the runs described here sufficient resolution was obtained with 40 mesh intervals in the z-direction but some runs were repeated with double that number. To measure the efficiency of convection we introduce a quadratic measure of the normalized superadiabatic heat transport, given by the Nusselt number

$$N = 2\langle \partial T/\partial z \rangle - 1, \tag{2.2}$$

	$\hat{\beta}$		N	P		$\hat{R}$		N
$\hat{R} = 2000$	256	TW	1.007		$\hat{\beta} = 8$	10800	TW	1.01
	128	TW	1.007			21600	TW	1.039
$\hat{R} = 4000$	64	SW	(1.12)	16.0		43200	TW	1.029
	32	SW	(1.12)	11.2		86400	TW	1.024
	16	SW	(1.10)	8.5				

TABLE 2. Weakly nonlinear behaviour: results for $\lambda = 2$. Bracketed values are averages.

where the angle brackets denote an average over the upper boundary. In the absence of convection $N = 1$.

3. Standing waves and travelling waves

Our aim is to map out the regions in parameter space where stable travelling waves can be found, paying particular attention to the associated bifurcations. The procedure is to obtain numerical solutions as $\hat{R}$ and $\hat{\beta}$ are varied systematically and to infer the bifurcation structure by reference to appropriate low-order models. (There is of course a risk that there may be more than one stable solution, as in §4.2 below.) We shall focus our attention on time-dependent nonlinear solutions with an aspect ratio $\lambda = 2$, corresponding to square rolls if mirror-symmetry is preserved, though the effects of varying the aspect ratio will be considered briefly. Figure 1 summarizes the behaviour we have found in different parts of the $(\hat{\beta}, \hat{R})$-parameter plane. The linear stability curves are also marked. From this figure we observe that stable travelling waves appear in three different regions: near the stability boundary, in a magnetically dominated regime; at intermediate field strengths, around $\hat{\beta} = 128$; and for weak fields at low Rayleigh numbers, around $\hat{R} = 2000$. We shall consider different aspects separately.

3.1. *Weakly nonlinear behaviour* ($\lambda = 2$)

We first investigate the transition between standing waves and travelling waves near the oscillatory bifurcation at $\hat{R} = \hat{R}^{(o)}$ in order to determine which solution is preferred. Thus we study marginal behaviour as $\hat{\beta}$ is decreased below the value at the Takens–Bogdanov bifurcation, where oscillations first appear. We find that solutions settle down rapidly to give either stable travelling waves or stable standing waves, regardless of initial conditions, without the uncertainties that arose with a vertical magnetic field in Part 1. The results of these runs are summarized in table 2.

The runs with $\hat{R} = 2000$ yield stable travelling waves. Perturbations to the trivial (static) solution develop into oscillations (standing waves) which gradually decay as the nonlinear solution converges to a travelling wave which is steady in a uniformly moving frame. Leftward- and rightward-travelling waves are exactly equivalent; which one appears depends on the initial conditions. Although the amplitude is small, the pattern is definitely asymmetric, as shown by the streaklines in figure 2(*a*). For this rightward-propagating wave the sinking plume is slanted in the rightward (prograde) direction. We might expect the pattern to travel horizontally as a slow magnetoacoustic wave, with a velocity given approximately by the Alfvén speed $\hat{v}_A$ at the middle of the layer (in the absence of diffusion); indeed it can be confirmed that, in the Boussinesq limit with σ, $\zeta \ll 1$, travelling waves first appear with a velocity

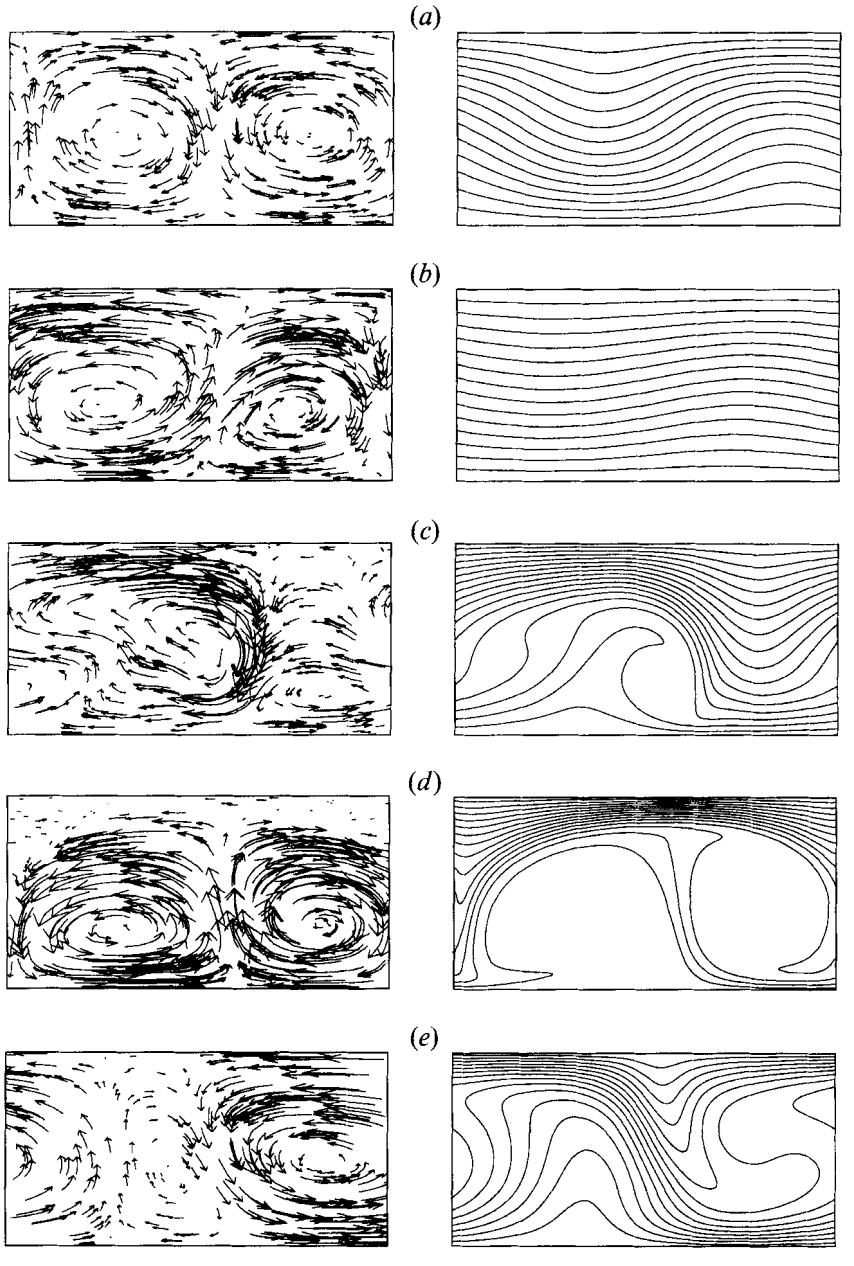

FIGURE 2. Different types of travelling waves. Streaklines of the velocity field (left) and magnetic field lines (right). Note the asymmetry of the streaklines. (*a*) Weakly nonlinear (propagating rightward with velocity $V = 0.076$, for $\hat{R} = 2000$, $\hat{\beta} = 128$). (*b*) The magnetically dominated regime (leftward with velocity $V = -0.306$, for $\hat{\beta} = 8$, $\hat{R} = 86400$). (*c*) The strong-field regime (leftward with $V = -0.114$, for $\hat{\beta} = 32$, $\hat{R} = 128000$). (*d*) The intermediate regime (rightward with $V = 0.051$, for $\hat{\beta} = 128$, $\hat{R} = 32000$). (*e*) The weak-field regime (leftward with $V = -0.065$, for $\hat{\beta} = 512$, $\hat{R} = 2000$).

that is equal to the Alfvén speed. For our reference atmosphere $\hat{v}_A = 2/(3\hat{\beta})^{1/2}$, so that $\hat{v}_A = 0.10$ for $\hat{\beta} = 128$. The wave in figure 2(*a*) travels at a somewhat lower velocity, owing principally to the effects of diffusion.

Since the value of $\hat{R}^{(o)}$ increases with increasing field strength, we have to choose a larger value of $\hat{R}$ in the strong-field regime. Hence we set $\hat{R} = 4000$ for $64 \geqslant \hat{\beta} \geqslant 16$. Here we only find stable standing wave solutions, with a pattern that is stationary in the frame with no net momentum. These solutions are mirror-symmetric about vertical planes with a separation $\frac{1}{2}\lambda$, centred on the rising and falling plumes, and the velocity reverses after half a period (cf. Weiss 1991; Proctor 1992).

For $\hat{\beta} < 16$ $\hat{R}^{(o)}$ increases rapidly and the stability boundary hugs the line $\hat{\beta} = 8$ in figure 1. (In fact, the critical value of $\hat{\beta}$ increases slightly when $R^{(o)}$ is large, as in figure 1(*b*) of Part 1.) We therefore set $\hat{\beta} = 8$ and obtain solutions as $\hat{R}$ is increased above the bifurcation point. For consistency, we choose the same values of $\hat{R}$ as in Part 1 and we find stable travelling waves once again. These solutions all have small amplitudes but the bifurcation appears to be subcritical. Figure 2(*b*) shows streaklines and field lines for a leftward-travelling wave: the magnetic field is only slightly disturbed but the asymmetry of the flow is much more pronounced than in figure 2(*a*). The large anticlockwise-rotating eddy contributes to a mean flow that is prograde near the top of the layer and retrograde at the bottom, with a jet in the retrograde direction. Once again the wave speed is somewhat less than the Alfvén speed ($\hat{v}_A = 0.41$).

Thus we find that weakly nonlinear solutions exhibit three different types of behaviour. Near the Takens–Bogdanov bifurcation, where we expect behaviour similar to that predicted in the Boussinesq approximation, travelling waves are indeed preferred and the solutions deviate only slightly from eigenfunctions of the linear problem. In the strong-field regime we find instead that standing waves are stable near the Hopf bifurcation but when the magnetic field is dominant (for $\hat{\beta} = 8$) we recover strongly asymmetric travelling waves. The latter differ in scale and appearance from the travelling wave solutions for $\hat{\beta} = 8$ in the presence of a vertical magnetic field, which are described in Part 1. However, it is characteristic of low-$\hat{\beta}$ behaviour, where the perturbed magnetic pressure is important, that travelling waves are preferred with either orientation of the field.

3.2. *The transition from standing waves to travelling waves ($\hat{\beta} = 32$)*

In the strong-field regime standing waves are initially preferred when $\lambda = 2$. As the Rayleigh number is increased, the standing waves lose stability in a pitchfork bifurcation, giving rise to modulated waves, which drift slowly while they oscillate. These waves gradually change in form as $\hat{R}$ is further increased, and develop into weakly modulated travelling waves. Eventually, stability is transferred to travelling waves in a Hopf bifurcation. Our results provide a particularly clear demonstration of this transition, though similar behaviour has been found in other problems. The bifurcation sequence can be established by reference to low-order evolution equations, which have already been discussed at length in Part 1.

We have explored the effects of increasing $\hat{R}$ for $\hat{\beta} = 32$ and the results are summarized in table 3. We first consider those obtained for $\lambda = 2$. At $\hat{R} = 4000$ we find the stable standing wave solution already mentioned but the standing waves then undergo a pitchfork bifurcation, at which their mirror symmetry is broken, giving rise to a pair of modulated waves, each of which is periodic, with period P, in a

	$\hat{R}$		N	P		$\hat{R}$		N	P
$\lambda = 1$	16000	TW	1.092		$\lambda = 3$	4000	SW	(1.11)	15.7
$\lambda = 1.5$	4000	SW	(1.05)	8.9		8000	MW	(1.16)	15.6
$\lambda = 2$	4000	SW	(1.12)	11.2		16000	QPMW	(1.26)	
	8000	MW	(1.22)	11.6		32000	MW	(1.30)	17.1
	16000	MW	(1.28)	12.2	$\lambda = 4$	4000	SW	(1.06)	20.5
	32000	MW	(1.30)	12.8					
	64000	MW	(1.35)	13.4					
	128000	TW	1.48						

TABLE 3. Standing waves and modulated waves: results for $\hat{\beta} = 32$.

slowly drifting frame. In this frame, the pattern repeats itself, with a displacement $\frac{1}{2}\lambda$, after an interval $\frac{1}{2}P$ in time. It is important to realize that there are two alternative ways of describing these modulated waves. The solution can be regarded either as a slowly drifting wave with period P and a symmetry with respect to translation by $\frac{1}{2}\lambda$ in x or as a modulated wave with a period $P' = \frac{1}{2}P$, travelling at a speed that is approximately λ/P (Proctor & Weiss 1993). This can be seen from figure 3(*a*), which shows a modulated wave for $\hat{R} = 8000$: clockwise-rotating eddies predominate over anticlockwise eddies at each phase of the cycle, giving rise to a horizontally averaged shear flow that is rightward at the top of the layer and leftward at the bottom. Near the pitchfork bifurcation it is natural to regard the wave as an asymmetric modulated standing wave with period P. We see that the eddies reverse and that over one period the pattern drifts slowly to the *right* with a velocity $V = 0.15\lambda/P$. (There is, of course, a mirror-image of this solution, which drifts to the left.) Alternatively, if we follow the sinking or rising plumes we find that the pattern of non-reversing eddies travels to the *left* with a velocity $V' = -0.85\lambda/P$ and a period P'.

As $\hat{R}$ is increased the modulated waves change in form and travel more rapidly, while their period increases. However, the time-averaged value of the Nusselt number changes very slowly, since the line of constant $\hat{\beta}$ in parameter space is never far from the line of Hopf bifurcations near $\hat{\beta} = 8$. Figure 3(*b*) shows a modulated wave for $\hat{R} = 64000$. This solution could be described as a pulsing travelling wave (cf. Landsberg & Knobloch 1993; Matthews *et al.* 1993). The dominant anticlockwise eddies drift to the right with a period P' and a velocity $V' = 0.40\lambda/P'$. The same solution can equivalently (if perversely) be regarded as a leftward drifting oscillation with the spatiotemporal symmetry described above, a period $P = 2P'$ and a velocity $V = -0.10\lambda/P'$.

The branch of travelling waves finally gains stability. Figure 2(*c*) shows a highly asymmetric solution for $\hat{R} = 128000$, which travels leftward without change of form. In contrast to the solution in figure 2(*b*), the large eddy is prograde at the bottom. The flow is strongly sheared, streaming in the retrograde direction at the top of the layer, but the Nusselt number is quite low, while magnetic flux is pumped towards the upper boundary. This solution has a very different structure from the weakly nonlinear travelling waves in figures 2(*a*) and 2(*b*).

We have also investigated the effect of varying the aspect ratio. For flatter cells with $\lambda = 3$, which are marginally favoured by linear theory, we again find standing waves, followed by modulated waves (at $\hat{R} = 16000$ the waves are quasi-periodically modulated). Standing waves again appear with $\lambda = 4$. As the aspect ratio is reduced,

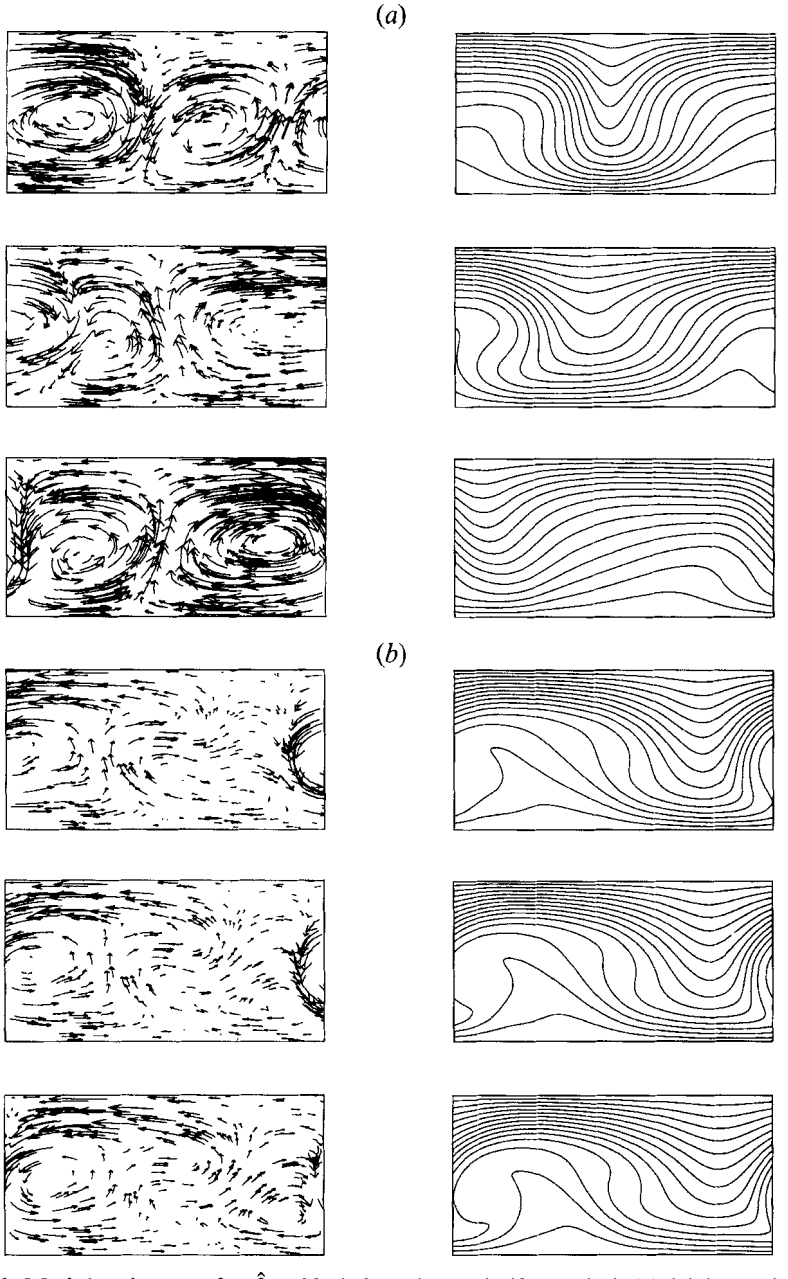

FIGURE 3. Modulated waves for $\hat{\beta} = 32$, followed over half a period. (*a*) Rightward drifting standing wave for $\hat{R} = 8000$. (*b*) Pulsing travelling wave for $\hat{R} = 64000$.

we find that standing waves are still preferred with $\lambda = 1.5$. The periods of these solutions are given approximately by the Alfvén crossing time $\lambda/\hat{v}_A$. It is only for narrow cells with $\lambda = 1$ that stable travelling waves finally appear. The value of $R^{(o)}$ is much higher for this aspect ratio and the solution at $\hat{R} = 16000$ settles down to a mildly asymmetric travelling wave. (This change in behaviour is caused by interactions between single roll and stacked roll solutions, which lead to streaming instabilities when the aspect ratio is small.)

$\hat{R}$		N	$\hat{R}$		N	P
2000	TW	1.0070	32000	PW	(2.31)	5.05
4000	TW	1.086	45000	MW	(2.5)	6.63
8000	TW	1.58	64000	PW	(2.55)	5.31
16000	TW	2.08	128000	PW	(2.70)	5.70
22500	TW	2.28	256000	Aperiodic	(2.8)	
32000	TW	2.39				

TABLE 4. The intermediate regime: results for $\hat{\beta} = 128$ with $\lambda = 2$.

This set of results for $\hat{\beta} = 32$ confirms that the qualitative behaviour found for $\lambda = 2$ is insensitive to the choice of aspect ratio; travelling waves can only be stabilized by forcing motion with $\lambda = 1$ and they become unstable if long-wavelength perturbations are admitted. Thus we are justified in confining our attention to solutions obtained with $\lambda = 2$. It is significant that, with a horizontal field, stable travelling waves do eventually appear when $\hat{R}$ is large; there are no indications of similar behaviour when the field is vertical.

3.3. *The intermediate regime* ($\hat{\beta} = 128$, $\lambda = 2$)

We next consider behaviour in the regime where the magnetic field is sufficiently strong for instability to set in at a Hopf bifurcation but $\hat{\beta}$ is not small enough for compressibility to be important. Since the layer is only weakly stratified, we expect to find behaviour similar to that predicted in the Boussinesq approximation, and travelling waves are indeed preferred in this regime, in contrast to behaviour when the field is vertical.

Results for $\hat{\beta} = 128$ are summarized in table 4. For $\hat{R} = 2000$ we obtain the stable travelling wave in figure 2(*a*), as might be anticipated from the analysis of Knobloch (1986), who showed that weakly nonlinear travelling waves were stable in the neighbourhood of the Takens–Bogdanov bifurcation for a Boussinesq fluid. As $\hat{R}$ is increased the travelling waves persist and become more asymmetric. We find stable travelling waves up to $\hat{R} = 32000$. The most significant feature of the rightward-propagating solution shown in figure 2(*d*) is the asymmetric distribution of magnetic flux, which is pumped upwards and concentrated near the top of the layer. The velocity pattern is not too different from that in figure 2(*a*), though there is a clear asymmetry, with a backward-tilted rising plume. The form of this solution is quite unlike that of the travelling wave for $\hat{\beta} = 32$ in figure 2(*c*), although the kinetic energy is only slightly less.

4. Travelling waves and steady convection ($\lambda = 2$)

In this section we study the interactions between travelling waves and steady convection, and interpret the behaviour found in numerical experiments by reference to the underlying bifurcation structure. In order to follow the transition from standing waves via modulated waves to travelling waves and then to a steady solution we decrease the imposed field for a fixed value of the Rayleigh number and identify the solutions that are stable in different regimes. By varying a single parameter we can construct a codimension-one bifurcation sequence. Repeating this process for different values of $\hat{R}$ then allows us to locate the bifurcation sets in a two-dimensional

	$\hat{\beta}$		N		N	
$\hat{R} = 1500$	1024	TW	1.126	SS	1.37	(transient)
	8192	TW	1.191	SS	1.54	
$\hat{R} = 2000$	512	TW	1.16	SS	1.57	(transient)
	1024	TW	1.14	SS	1.77	
	2048	TW	1.132	SS	1.84	
	4096	TW	1.130	SS	1.87	
	8192	TW	1.130	SS	1.89	
	2^{14}	TW	1.129	SS	1.89	
$\hat{R} = 4000$	256			SS	1.96	
	512			SS	2.42	
$\hat{R} = 32000$	16	QPMW	(1.25)			
	32	MW	(1.30)			
	64	QPMW	(1.48)			
	128	TW	2.39			
	256	TW	3.10			
	512			SS	4.11	

TABLE 5. Travelling waves and steady convection: results for $\lambda = 2$.

$(\hat{\beta}, \hat{R})$-parameter plane. As expected, the Takens–Bogdanov bifurcation, which is of codimension two, plays an important role as an organizing centre in this plane. The results are summarized in table 5: for moderate Rayleigh numbers ($\hat{R} = 4000$, 32000) the associated bifurcation structure is relatively simple but behaviour at low Rayleigh numbers ($\hat{R} = 1500$, 2000) proves more complicated, owing to the proximity of the Takens–Bogdanov bifurcation and to the survival of travelling waves even in the absence of a magnetic field.

4.1. *Bifurcation from the steady solution*

We first consider the sequence of solutions obtained for $\hat{R} = 4000$ as the imposed field is reduced below the value at the Hopf bifurcation from the trivial solution. Near the bifurcation we find stable standing waves which persist, as described in §3.1 above, until there is a transition to stable travelling waves and thence to stable steady convection for $\hat{\beta} \geqslant 256$. Steady solutions actually appear before the pitchfork bifurcation, as expected from Arter's (1983) study of the Boussinesq problem, and then remain stable through the weak-field regime; however, our results differ from Arter's owing to the adoption of periodic lateral boundary conditions, which allow a new branch of travelling waves to appear. The corresponding bifurcation pattern is sketched in figure 4(*a*). The structure here, and in subsequent figures, is minimal: the existence of all the bifurcations and solution branches that are shown can be deduced from the numerical experiments but, since the unstable solutions cannot be computed, there may be further bifurcations on the unstable branches. Although its general structure resembles that for a vertical field (cf. figure 4(*a*) of Part 2) the travelling waves are stable over a much wider range when the field is horizontal.

At higher values of $\hat{R}$ the standing waves are always unstable. Figure 4(*b*) shows the bifurcation pattern for $\hat{R} = 32000$. Travelling waves are preferred in the weakly nonlinear regime but then lose stability to modulated waves which undergo a further Hopf bifurcation to give quasi-periodic modulation with intervals of frequency locking. (Behaviour at $\hat{\beta} = 64$, where there is very slow modulation of a double-humped basic cycle, suggests that there is some interaction with the pulsating waves to be

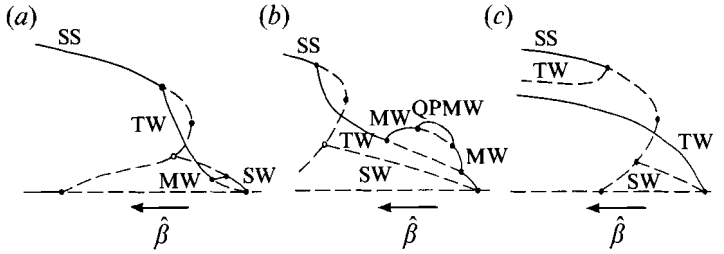

FIGURE 4. Travelling waves and steady convection: schematic bifurcation patterns, showing N as a function of $\hat{\beta}$. (*a*) For $\hat{R} = 4000$: the branch of SS which emerges from the stationary bifurcation at $\hat{\beta}^{(e)} = 340$ has a turning point at $\hat{\beta} \approx 180$, giving rise to subcritical steady convection. Branches of SW and TW solutions emerge together from the oscillatory bifurcation at $\hat{\beta}^{(o)} = 11$. The SW branch terminates in a heteroclinic bifurcation on an unstable segment of the steady branch, while the TW branch joins the steady branch in a pitchfork bifurcation. SW are stable for $\hat{\beta}^{(o)} < \hat{\beta} \lesssim 90$; then stability is transferred to TW via a short branch of MW (which we have not explicitly located) and the TW finally give way to steady convection at $\hat{\beta} \approx 200 < \hat{\beta}^{(e)}$. The SS remain stable as $\hat{\beta} \to \infty$. (*b*) For $\hat{R} = 32000$: TW are stable near the Hopf bifurcation at $\hat{\beta}^{(o)} = 8$ but undergo further Hopf bifurcations to give quasi-periodic MW. Frequency locking leads to solutions that are periodic in a moving frame, at a 1:24 resonance for $\hat{\beta} = 16$ and a 1:1 resonance for $\hat{\beta} = 32$ but the solution at $\hat{\beta} = 64$ is quasi-periodic in the moving frame. The branch of TW regains stability at $\hat{\beta} \approx 100$ and joins the steady branch at $\hat{\beta} \approx 300$. (*c*) For $\hat{R} = 2000$, showing two branches of TW, emerging from the primary Hopf bifurcation and from a secondary pitchfork bifurcation. The steady branch emerges from a pitchfork bifurcation ($\hat{\beta}^{(e)} = 470$) and has a turning point at $\hat{\beta} \approx 400$, but SS only gain stability in a subcritical pitchfork bifurcation, at $\hat{\beta} \approx 800$, which gives rise to unstable TW. The branch of stable TW that emerges from the Hopf bifurcation persists for all $\hat{\beta} > \hat{\beta}^{(o)} = 71$, while the unstable SW branch ends in a heteroclinic bifurcation.

described in §5.) The branch of travelling waves eventually regains stability and joins the steady branch as before.

4.2. *The weak-field regime*

From figure 1 we observe that stable travelling waves appear at low Rayleigh numbers in a band around $\hat{R} = 2000$ that covers the multiple bifurcation at $\hat{\beta} = 495$ and persists into the kinematic regime as $\hat{\beta} \to \infty$. Evidently the bifurcation structure has features that are more subtle than would appear from figure 4.

As the field strength is decreased with $\hat{R} = 2000$ stable TW first appear near the Hopf bifurcation at $\hat{\beta}^{(o)} = 68$, as described in §3.1. The solution for $\hat{\beta} = 128$ was illustrated in figure 2(*a*). Figure 2(*e*) shows a travelling wave at $\hat{\beta} = 512$, close to the Takens–Bogdanov point. Motion is dominated by a single eddy which produces a mean shear flow with a prograde velocity at the upper boundary. Magnetic flux is concentrated at the top and bottom of the layer and in the region where the flow is weak, but the field is strongest near the upper boundary. The Nusselt number for this solution is actually greater than that for $\hat{\beta} = 256$: apparently the bifurcation has become subcritical. By using solutions computed at lower $\hat{\beta}$ to provide initial conditions slowly travelling waves can be followed into the weak-field regime, where there is only a stationary bifurcation from the trivial solution. As the field strength is decreased to a value that is negligibly small (see table 6) the solutions remain stable and similar to that in figure 2(*e*). Stable steady solutions can also be obtained, by perturbing an initially static configuration. Like SW, these solutions have mirror

	$\hat{R}$		N		$\hat{R}$		N
$\hat{\beta} = 2^{20}$	2000	TW	1.13	$Q = 0.108$	1000	SS	1.062
		SS	1.90				
	4000	SS	2.75		1500	TW	1.119
						SS	1.56
	8000	SS	3.60		2000	TW	1.13
						SS	1.90
	16000	SS	4.63		2500	SS	2.15
	32000	SS	5.80		3000	SS	2.37
	64000	PW(QP)	(7.3)		4000	SS	2.70

TABLE 6. The kinematic limit: results for $\lambda = 2$.

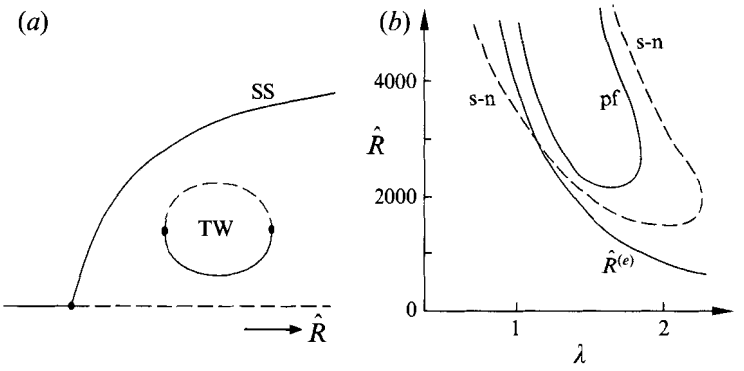

FIGURE 5. Travelling waves in the weak-field regime. (*a*) Bifurcation pattern as $\hat{R}$ is increased when Q is very small, showing the bubble of TW. With suitably chosen initial conditions we obtain stable TW for $\hat{R} = 1500$ and 2000. Using these TW as initial conditions for runs with $\hat{R} = 1000$, 2500, we recover SS. We have also confirmed that SS at $\hat{R} = 1500$, 2000 are stable to TW perturbations. (*b*) Origin of the bubble: conjectured bifurcations in the $(\lambda, \hat{R})$-plane for $Q = 0$, showing bifurcations from the trivial solution ($\hat{R} = \hat{R}^{(e)}$), pitchfork bifurcations from SS to TW (full line) and saddle-node bifurcations of TW (broken line).

symmetry about vertical planes. Solutions with $\hat{\beta} \geqslant 1024$ are found to be stable to TW perturbations. At $\hat{\beta} = 512$, however, we find a transient SS that gives way to TW. At this point in parameter space, only travelling waves are stable.

Both TW and SS can also be found with $\hat{R} = 1500$. The trivial solution is stable for $\hat{\beta} \leqslant 633$ but for $\hat{\beta} = 1024$ we obtain a transient steady state that gives way to a stable TW. From it we obtain TW for larger values of $\hat{\beta}$. Steady solutions can also be obtained for the same parameter values.

In order to understand the behaviour revealed by these results we have proceeded towards the kinematic limit and computed solutions as $\hat{R}$ is varied with a field that is negligibly small. Following Part 2, we set $Q = 0.108$ (corresponding to $\hat{\beta} = 2^{20}$ at $\hat{R} = 8000$) and obtain the results listed in table 6. The steady branch that emerges from the primary pitchfork bifurcation is stable to TW perturbations at least for $\hat{R} \leqslant 8000$, while two branches of TW (one stable, the other unstable) appear in a saddle-node bifurcation at $\hat{R} \approx 1200$ and disappear in another at $\hat{R} \approx 2200$, as sketched in figure 5(*a*). Although these TW are a purely hydrodynamic phenomenon,

it would be difficult to reach them without starting from magnetically generated TW solutions.

In any nonlinear problem there is always a risk that new solutions may appear in an isolated bubble between a pair of saddle-node bifurcations. This may be tiresome but if it happens one should seek some plausible explanation. Let us therefore briefly consider the two-parameter problem where both λ and $\hat{R}$ are varied for $Q = 0$. When $\hat{R}$ is increased for $\lambda = 1$ the steady branch sheds TW in a subcritical pitchfork bifurcation close to the stationary bifurcation at $\hat{R}^{(e)} = 3204$ (see Part 2). We conjecture that subcritical pitchfork bifurcations from the symmetrical steady solutions lie on a curve in the $(\lambda, \hat{R})$-plane with a turning point at some λ_0 ($1 < \lambda_0 < 2$), as indicated in figure 5(*b*). Thus the pitchfork bifurcations do not occur for $\lambda > \lambda_0$. The curve on which they lie is enclosed by a curve of saddle-node bifurcations that intersects the line $\lambda = 2$ twice, as described above, and probably even extends to $\lambda = 4$ (cf. Part 2). Thus the bubble at $\lambda = 2$ is not completely isolated; rather, it is linked to bifurcations from SS at smaller aspect ratios.

For $\lambda = 2$ the bubble intersects the steady branch again if the magnetic field is sufficiently strong. The overall bifurcation pattern for $\hat{R} = 2000$ is sketched in figure 4(*c*). The steady branch undergoes a saddle-node bifurcation but only gains stability in the subcritical pitchfork bifurcation, shedding a pair of unstable TW which remain as $\hat{\beta} \to \infty$. Meanwhile, the branch of stable TW that emerges from the primary Hopf bifurcation persists for all $\hat{\beta} > \hat{\beta}^{(o)}$. This bifurcation pattern differs significantly from that for a vertical field (see figure 3(*a*) of Part 2). When the field is vertical TW are only stable for a narrow range ($1024 \geqslant \hat{\beta} \geqslant 512$) with $\hat{R} = 2000$. Moreover, the pitchfork bifurcation from SS at $\hat{\beta} \approx 1500$ is supercritical and there is no link to the bubble of TW in the kinematic regime.

The lower part of figure 6(*a*) shows the bifurcation set in the $(\hat{\beta}, \hat{R})$-plane that corresponds to figures 4(*c*) and 5(*a*). The line of primary pitchfork bifurcations ($\hat{R} = \hat{R}^{(e)}$) intersects the line of primary Hopf bifurcations ($\hat{R} = \hat{R}^{(o)}$) at the Takens–Bogdanov point. Near that point the latter bifurcation is subcritical, so that there is a saddle-node bifurcation at the turning point on the TW branch. When the field is significant there is also a line of saddle-node bifurcations ($\hat{R} = \hat{R}_{\min}$) on the steady branch. Travelling waves bifurcate from the steady branch on a line of secondary pitchfork bifurcations which curves out of the Takens–Bogdanov point and extends to large $\hat{R}$ (see below). For $\hat{R} > 2200$ the pitchfork bifurcations are supercritical but for $2200 \geqslant \hat{R} \geqslant 1300$ they become subcritical. Consequently there are two lines of saddle-node bifurcations of TW, which extend to the kinematic limit. These lines define the band of stable TW in the weak-field regime.

4.3. *Travelling waves and the Takens–Bogdanov bifurcation*

The region near the double-zero Takens–Bogdanov bifurcation in figure 6(*a*) is enlarged in figure 6(*b*) to show more detail. Behaviour here is more complicated still. The line of secondary pitchfork bifurcations curves round the Takens–Bogdanov point and touches the line of saddle-node bifurcations on the steady branch. At the point of tangency the pitchfork bifurcation from SS to TW is transferred from the upper to the lower segment of the steady branch. Since the amplitude of TW solutions for $\hat{R} = 2000$ increases towards the Takens–Bogdanov point, the Hopf bifurcation must become subcritical; the line of saddle-node bifurcations on the TW branch is indicated in figure 6(*b*).

The codimension-one bifurcation sequence along the slice labelled (i) in figure 6(*b*)

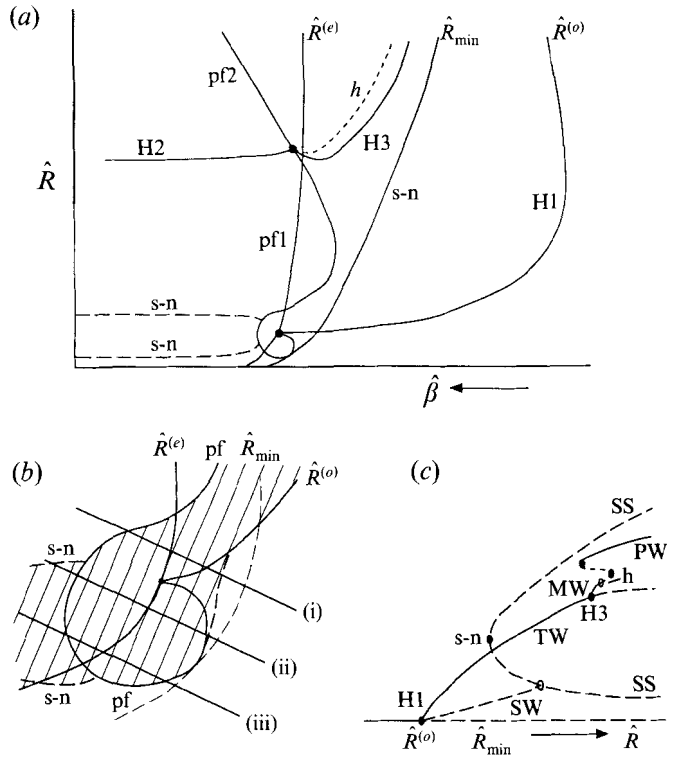

FIGURE 6. (*a*) Bifurcations in the $(\hat{\beta}, \hat{R})$-plane, showing the lines of primary Hopf (H1) and pitchfork (pf1) bifurcations, at $\hat{R}^{(o)}$ and $\hat{R}^{(e)}$, emerging from the lower Takens–Bogdanov point, and the line of turning points on the steady branch at $\hat{R}_{\min}$. Also shown are the lines of secondary pitchfork bifurcations to TW (labelled pf2), and the lines of saddle-node bifurcations of TW solutions (labelled s-n). From the upper Takens–Bogdanov point there emerges a line of secondary Hopf bifurcations (H2) that gives rise to PW, together with a line of tertiary Hopf bifurcations (H3) leading to MW and a line of gluing bifurcations (h) that produces PW. (*b*) Detail showing behaviour near the lower Takens–Bogdanov point. TW exist within the shaded region. (*c*) Transitions from travelling waves to pulsating waves: bifurcations as $\hat{R}$ is increased for $\hat{\beta} = 128$, showing transitions from TW to MW and PW. The TW branch emerges from the primary Hopf bifurcation (H1) and undergoes a subsequent Hopf bifurcation (H3) that gives rise to MW, which acquire spatiotemporal symmetry at a gluing bifurcation (h) that leads to PW.

is sketched in Figure 7(*a*). Here the branch of TW is stable between the turning point and the supercritical pitchfork bifurcation from the steady branch. The slice labelled (ii) lies beyond the Takens–Bogdanov point: although the primary Hopf bifurcation has disappeared, TW emerge from a secondary pitchfork bifurcation which gradually climbs up the unstable segment of the steady branch. The corresponding bifurcation diagram in figure 7(*b*) shows that TW are stable on a segment that lies between two saddle-node bifurcations, since the upper pitchfork has become subcritical. Finally, figure 7(*c*) shows bifurcations along the slice labelled (iii). Now the secondary bifurcation has moved round the turning point on the steady branch and there is a short, stable section near the saddle-node. TW are stable between the secondary pitchfork and the saddle-node that precedes the subcritical tertiary pitchfork. Apart from that last bifurcation the structure is similar to that found when the field is vertical (cf. Part 2). Analogous behaviour for standing waves has been described by Rucklidge *et al.* (1993). The normal form equations for a Takens–Bogdanov bifurcation with

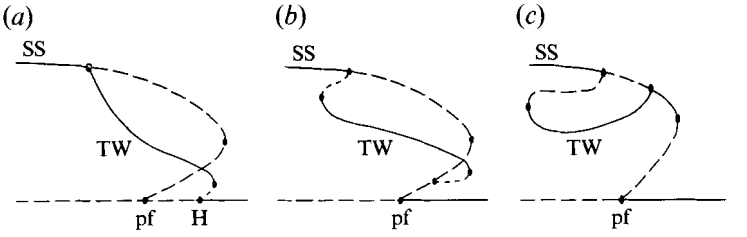

FIGURE 7. TW and SS: bifurcations along the cuts labelled (i), (ii), (iii) in figure 6(*b*).

$O(2)$ symmetry (Dangelmayr & Knobloch 1987) need to be augmented by including higher-order terms in order to cover the behaviour described here; the resulting system will be discussed elsewhere.

5. Pulsating waves ($\lambda = 2$)

The steady solutions are mirror-symmetric about vertical planes, separated by $\frac{1}{2}\lambda$ and centred on rising and falling plumes. This symmetry may be broken in two ways. A pitchfork bifurcation leads to uniformly drifting travelling waves, as described in §4; but a Hopf bifurcation gives rise to pulsating waves, which possess a spatiotemporal symmetry corresponding to reflection about a mirror-plane after translation by half a period in time (Landsberg & Knobloch 1991; Proctor & Weiss 1993). Streaming instabilities provide an alternative route to pulsating waves: as $\hat{R}$ is increased, travelling waves may lose stability to modulated waves, which are transformed into pulsating waves at a global gluing bifurcation (Matthews *et al.* 1993). We find examples of both routes.

Pulsating waves are particularly prominent when the field is vertical and they are discussed in greater detail in Part 2. Lantz & Sudan (1995) and Lantz (1995) have investigated the transition from steady convection to pulsating waves in a horizontal field. They used the anelastic approximation and adopted different magnetic boundary conditions, with B_x fixed at $z = z_0 + 1$ and $\boldsymbol{B}$ matched to a potential field at $z = z_0$. In their computations the aspect ratio was small ($\lambda = 1$). As Q was decreased for fixed $\hat{R}$ they found a transition from SS to PW and thence to TW and, eventually, to MW. Their results could also be related to earlier calculations with $Q = 0$ (Ginet & Sudan 1987).

We shall consider wider cells, with $\lambda = 2$ so that rolls have a square cross-section in the steady state. For intermediate fields, we find some novel and complicated behaviour. As we have seen, travelling waves are preferred at low $\hat{R}$ when $\hat{\beta} = 128$. In fact, we obtain stable TW for $2000 \leqslant \hat{R} \leqslant 32000$. However, the travelling waves become unstable for $\hat{R} \geqslant 45000$: over the range $32000 \leqslant \hat{R} \leqslant 128000$ we find stable pulsating waves, with Nusselt numbers that oscillate with increasing amplitude about a mean value slightly lower than that for the TW. The velocity and magnetic field for a PW at $\hat{R} = 64000$ are illustrated in figure 8. The rising plume waggles alternately to left and right, so that after half a period $\boldsymbol{u}$ and $\boldsymbol{B}$ are reflected about mirror-planes. At yet higher Rayleigh numbers the PW become chaotic; so at $\hat{R} = 256000$ we only find aperiodically pulsating waves.

There is thus a range with hysteresis, where both travelling and pulsating waves are stable. In Part 2 we found that the transition from TW to PW involved an intermediate branch of modulated waves, and indeed we find here that at $\hat{R} = 45000$

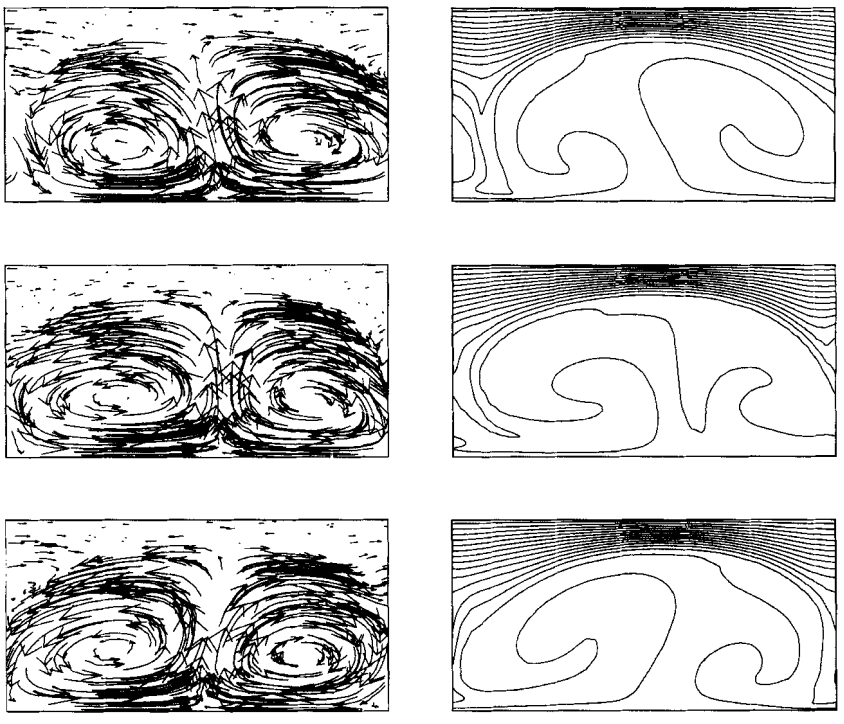

FIGURE 8. Pulsating wave for $\hat{\beta} = 128$, $\hat{R} = 64000$, showing solutions at intervals of a quarter-period. The first and last are related by the broken mirror symmetry.

the TW loses stability and gives way to a stable MW. The wave is only slightly asymmetric, while the modulation has a longer period than the PW and is weak. These results permit the construction of the minimal bifurcation diagram shown in figure 6(*c*), which is consistent with all the known behaviour at $\hat{\beta} = 128$.

In Part 2 we described a low-order model (Rucklidge & Matthews 1993, 1995) in which such transitions were related to a multiple (Takens–Bogdanov) bifurcation from the steady solution, which acted as an organizing centre in the $(\hat{R}, Q)$-plane. There are several items of evidence suggesting that the behaviour shown here may be related to the presence of a (degenerate) Takens–Bogdanov bifurcation from the SS solution, not far away in the $(\hat{\beta}, \hat{R})$-plane. First of all, as we have seen, the TW and PW resemble the SS solutions closely with small asymmetry and low phase velocities, all suggesting the presence nearby of a pitchfork bifurcation from SS to TW and a Hopf bifurcation from SS to PW. Indeed, we already know that there is a line of pitchfork bifurcations to TW that passes between $\hat{\beta} = 512$ and $\hat{\beta} = 256$ for $\hat{R} = 32000$ (cf. figure 1). There is also evidence for a line of secondary Hopf bifurcations from SS to PW extending from the Takens–Bogdanov point to large $\hat{\beta}$. Results for $\hat{\beta} = 2^{20}$, given in table 6, show that (as already mentioned in §4.2) steady solutions remain stable up to $\hat{R} = 32000$. Convection at $\hat{R} = 64000$ displays quite different behaviour. Mirror-symmetry is broken and the time-dependent solution oscillates about the unstable SS. We infer that there is a Hopf bifurcation, around $\hat{R} = 50000$, that gives rise to pulsating waves. Close inspection of our solution at $\hat{R} = 64000$ reveals that it is actually quasi-periodic, with a weak but definite modulation (apparently near a period-doubling resonance). Although this result can

only be regarded as suggestive, since our numerical resolution is inadequate at this Rayleigh number, we believe that it is qualitatively reliable. The computational difficulties become apparent when we calculate the peak local value, $M_{\max}$, of the Mach number, $M = |\boldsymbol{u}|/v_s$, where $v_s^2 = \gamma T$. When $\hat{\beta} = 128$, the velocity is everywhere subsonic, with $M_{\max} \leqslant 0.67$, owing to the presence of a significant magnetic field. In the kinematic limit, we find, however, that $M_{\max} > 1$ for $\hat{R} \geqslant 2000$; the regions where the flow is supersonic are highly localized, near the upper boundary (where T is small) and in the sinking plumes. Our difference scheme cannot describe shocks and local structures must be affected by discretization as $M_{\max}$ increases. To estimate the effect of discretization errors we repeated the run at $\hat{R} = 32000$ with doubled resolution and found no change in N, with a 3% decrease in $M_{\max}$; these global quantities apparently remain insensitive to truncation errors at this value of $\hat{R}$. In fact, precise computations by Cattaneo, Hurlburt & Toomre (1990) show that shocks develop at high $\hat{R}$, giving rise to aperiodic oscillatory behaviour. We presume that the oscillations appear first as PW and that subsequent bifurcations lead to chaos.

We thus infer the bifurcation structure in the upper part of figure 6(*a*). The new Takens–Bogdanov point, with $\hat{R} \approx 50000$, acts as an organizing centre. From it emerge lines of secondary pitchfork bifurcations from the SS branch, of secondary Hopf bifurcations as described above, tertiary Hopf bifurcations leading to MW, and gluing bifurcations giving the PW. Other lines of saddle-node bifurcations will also be present. Fortunately it is not necessary to analyse all the details as the picture is consistent with one of the unfoldings of the Takens–Bogdanov bifurcation with a subcritical Hopf bifurcation branch (requiring additional quintic terms for completeness), which has already been discussed by Rucklidge *et al.* (1993) in another context. The structure near the Takens–Bogdanov point is similar to that in their figure 4, while their figure 5(*b*) shows a pair of saddle-node bifurcations corresponding to those on the PW branch in our figure 6(*c*).

The pulsating waves described here are relatively tame; the interesting feature is their relationship to travelling waves. When the aspect ratio is reduced, streaming instabilities lead to more dramatic oscillations, which arise both when the field is horizontal (Lantz & Sudan 1995) and when it is vertical (see Part 2). The associated bifurcation structure can be clarified by reference to suitable low-order models. Lantz (1995) constructed a ninth-order system that represents the transition from SS to TW and thence to MW and PW, while Rucklidge & Matthews (1993, 1995; Matthews *et al.* 1993) have developed a fifth-order model and analysed its bifurcation structure in great detail. Since this topic has already been treated in Part 2, we shall not pursue it here.

6. Discussion

This study clearly demonstrates that any interpretation of numerical experiments on nonlinear convection must rely on establishing the appropriate bifurcation structure. For our idealized problem, we have succeeded in isolating the various regimes in which different types of travelling wave are stable. In addition, we have investigated the web of relationships between travelling waves and steady solutions, standing waves, modulated waves and pulsating waves, and unravelled the bifurcation sequences in each regime. The results of our numerical experiments are summarized in figure 1, while the relevant bifurcation structures are displayed in figure 6(*a*). The latter is dominated by the presence of two Takens–Bogdanov bifurcations, each of

codimension two, which act as organizing centres in the $(\hat{\beta}, \hat{R})$-parameter plane. It is apparent that no single process can explain the occurrence of travelling waves in different regions of this plane. Indeed, a summary of our results confirms that several different mechanisms are involved.

In the magnetically dominated regime TW are preferred to SW. For $\hat{\beta} = 8$, near the stability boundary, only TW are found. They are apparently driven by fluctuations in magnetic pressure which, as in the case of a vertical field, cannot readily be balanced by thermal pressure in this low-$\hat{\beta}$ limit. In a horizontal field we might expect these waves to travel as slow magnetoacoustic waves with a velocity close to the Alfvén speed. For our configuration ($\hat{\beta} = 8$, $\lambda = 2$) slow waves would propagate horizontally with a velocity $V = 0.96\hat{v}_A$ but fast waves would have $V = 3.80\hat{v}_A$; for the example in figure 2(*b*) the actual wave speed $V = 0.75\hat{v}_A$. There are significant differences from the results reported for a vertical field in Part 1. In the latter case the TW all had a wavelength $\lambda = 1$ and were unstable in the immediate neighbourhood of the Hopf bifurcation for $\hat{\beta} = 8$. Here stable TW appear immediately with $\lambda = 2$. Moreover, the solutions have a very different structure. Whereas the TW in Part 1 have a triangular form with a prograde jet, the rolls in figure 2(*b*) are distinctly asymmetric, with a retrograde jet. The sense of the more prominent eddy is such that motion is prograde at the top of the layer.

SW are preferred near the oscillatory bifurcation in the strong-field regime ($16 \leqslant \hat{\beta} \leqslant 64$). The behaviour of weakly nonlinear convection is similar to that found when the field is vertical but there is a profound difference at large $\hat{R}$, where TW acquire stability. Moreover, these TW (in figure 2*c*) have a different form from those in the magnetically dominated regime: they are very asymmetric but the prominent eddy is prograde at the bottom, while magnetic flux is pumped towards the top of the layer.

Since our layer is only weakly stratified we expect to find behaviour consistent with Boussinesq theory at intermediate field strengths ($128 \leqslant \hat{\beta} \leqslant 256$), when compressibility is less important. This is the regime where TW are preferred at onset, in contrast to behaviour when the field is vertical. The solution in figure 2(*a*), near the initial bifurcation, resembles the eigenfunction of the linear problem. Even at a higher Rayleigh number the drifting rolls in figure 2(*d*) are only mildly asymmetric; the prominent eddy is again prograde at the bottom while flux is concentrated near the top of the layer, where motion is suppressed. This vertical asymmetry suggests that the stratification has become significant. In this regime the difference between vertical and horizontal fields is quite clear. Travelling waves are favoured in the latter case and persist to relatively high values of $\hat{R}$ – where they only disappear as a result of further instabilities associated with streaming flows.

Travelling waves also persist beyond the bifurcation of codimension two with $\hat{\beta} = 495$. The convoluted bifurcation structure in figure 6(*b*) arises when the primary bifurcation to TW is subcritical in the neighbourhood of this Takens–Bogdanov bifurcation. Thus we expect to find TW at low Rayleigh number for $\hat{\beta} = 512$, 1024. Indeed, TW also appear in this region when the field is vertical. Their occurrence here is a consequence of nonlinear dynamics rather than of any specific physical mechanism.

Finally we come to the weak-field regime, where TW exist for $1500 \leqslant \hat{R} \leqslant 2000$. The wave for $\hat{\beta} = 512$ in figure 2(*e*) is different again: the rolls are strongly asymmetric but the prominent eddy is prograde at the top and there is no significant pumping of magnetic flux. This structure is preserved as $\hat{\beta} \to \infty$ though the asymmetry becomes

more marked, until the subsidiary eddy almost disappears; meanwhile, the velocity remains small and scarcely changes. These TW are purely hydrodynamic in origin: they are caused by a tilting instability that gives rise to shear (Howard & Krishnamurti 1986; Matthews *et al.* 1993). The only difference between vertical and horizontal fields is that the TW are always present in the latter case.

There is no single simple answer to the question: what mechanism determines whether SW or TW are preferred? Near the initial Hopf bifurcation the coefficients of the relevant terms in a centre manifold reduction depend on a delicate balance between competing processes and the result cannot readily be predicted (Matthews & Rucklidge 1993). The preference for TW near the stability boundary at $\hat{\beta} = 8$ is due to compressibility. In the strong-field regime SW are initially preferred for either orientation of the field, though TW eventually take over when the field is horizontal. With weak fields, the steady state is stable but stratification allows stable TW to appear as a hydrodynamic effect. It is only for intermediate field strengths, in an effectively Boussinesq regime, that there is a striking difference between vertical and horizontal fields, as suggested by weakly nonlinear theory (Dangelmayr & Knobloch 1986; Knobloch 1986). Here we find that SW are preferred when waves travel up and down along a vertical field, while TW are stable when the field is horizontal.

The overall comparison between figure 1 of this paper and figure 2(*a*) of Part 1 certainly indicates that stable TW are more prevalent with a horizontal field. This accords with our intuitive expectation that travelling waves should be favoured when they can propagate horizontally as slow magnetoacoustic waves. In this context, it is significant that in thermosolutal convection, where disturbances travel obliquely, TW are again preferred (Moore & Weiss 1990). The general conclusion to be drawn from these idealized model calculations is that travelling waves of one kind or another can be excited convectively when the field is strongly inclined, as in the penumbra of a sunspot. There is an obvious example of this process. Running penumbral waves propagate radially outwards across the penumbra and extend coherently over a large azimuthal angle (Lites 1992); they seem to be unaffected by the fine-scale filamentary structure. These waves are observed in the chromosphere and upper photosphere, and travel at (or faster than) the sound speed. They can be modelled as fast magneto-atmospheric waves, trapped in a low-velocity layer, since the Alfvén speed increases upwards into the chromosphere and the sound speed increases downwards below the photosphere. Such waves can obviously be excited by the superadiabatic stratification and so it is likely that they too have a convective origin (Thomas & Weiss 1992).

This paper concludes our investigations of two-dimensional magnetoconvection. We have successfully isolated different types of oscillatory behaviour and analysed their properties. Together with the pioneering study of Hurlburt & Toomre (1988) this series extends the systematic treatment of Boussinesq magnetoconvection (Proctor & Weiss 1982) to include effects of compressibility and of relaxing lateral boundary conditions. We have found standing waves, travelling waves, pulsating waves and modulated waves in vertical and horizontal fields. The next stage is to tackle the more realistic problem of three-dimensional magnetoconvection. Preliminary results (Matthews 1993; Matthews *et al.* 1994) confirm that similar solutions can be found, together with a rich variety of new phenomena. Unravelling the associated bifurcation structures will provide a challenge for the future.

We are grateful for comments from Paul Matthews and Alastair Rucklidge, and for exchanges of information with Steven Lantz. This work was supported by grants from SERC.

REFERENCES

ARTER, W. 1983 Nonlinear convection in an imposed horizontal magnetic field. *Geophys. Astrophys. Fluid Dyn.* **25**, 259–292.

CATTANEO, F. 1984 Compressible magnetoconvection. PhD Dissertation, University of Cambridge.

CATTANEO, F., HURLBURT, N. E. & TOOMRE, J. 1990 Supersonic convection. *Astrophys. J.* **349**, L63–L66.

CHANDRASEKHAR, S. 1961 *Hydrodynamic and Hydromagnetic Stability*. Clarendon Press.

DANGELMAYR, G. & KNOBLOCH, E. 1986 Interaction between standing and travelling waves and steady states in magnetoconvection. *Phys. Lett.* A **117**, 394–398.

DANGELMAYR, G. & KNOBLOCH, E. 1987 The Takens–Bogdanov bifurcation with $O(2)$ symmetry. *Phil. Trans. R. Soc. Lond.* A **322**, 243–279.

GINET, G. P. & SUDAN, R. N. 1987 Numerical observations of dynamical behavior in two-dimensional compressible convection. *Phys. Fluids* **30**, 1667–1677.

HOWARD, L. N. & KRISHNAMURTI, R. 1986 Large-scale flow in turbulent convection: a mathematical model. *J. Fluid Mech.* **170**, 385–410.

HURLBURT, N. E., MATTHEWS, P. C. & PROCTOR, M. R. E. 1995 Nonlinear compressible convection in oblique magnetic fields. *Astrophys. J.* (in press).

HURLBURT, N. E., PROCTOR, M. R. E., WEISS, N. O. & BROWNJOHN, D. P. 1989 Nonlinear compressible magnetoconvection. Part 1. Travelling waves and oscillations. *J. Fluid Mech.* **207**, 587–628.

HURLBURT, N. E. & TOOMRE, J. 1988 Magnetic fields interacting with nonlinear compressible convection. *Astrophys. J.* **327**, 920–932.

KNOBLOCH, E. 1986 On convection in a horizontal magnetic field with periodic boundary conditions. *Geophys. Astrophys. Fluid Dyn.* **36**, 161–177.

LANDSBERG, A. S. & KNOBLOCH, E. 1991 Direction-reversing traveling waves. *Phys. Lett.* A **159**, 17–20.

LANDSBERG, A. S. & KNOBLOCH, E. 1993 New types of waves in systems with $O(2)$ symmetry. *Phys. Lett.* A **179**, 316–319.

LANTZ, S. R. 1995 Magnetoconvection dynamics in a stratified layer. II. A low-order model of the tilting instability. *Astrophys. J.* **441**, 925–941.

LANTZ, S. R. & SUDAN, R. N. 1995 Magnetoconvection dynamics in a stratified layer. I. 2D simulations and visualization. *Astrophys. J.* **441**, 903–924.

LITES, B. W. 1992 Sunspot oscillations: observations and implications. In *Sunspots: Theory and Observations* (ed. J. H. Thomas & N. O. Weiss), pp. 261–302. Kluwer, Dordrecht.

MATTHEWS, P. C. 1993 Compressible magnetoconvection in three dimensions. In *Theory of Solar and Planetary Dynamos* (ed. M. R. E. Proctor, P. C. Matthews & A. M. Rucklidge), pp. 211–218. Cambridge University Press.

MATTHEWS, P. C., HURLBURT, N. E., PROCTOR, M. R. E. & BROWNJOHN, D. P. 1992 Compressible magnetoconvection in oblique fields: linearized theory and simple nonlinear models. *J. Fluid Mech.* **240**, 559–569.

MATTHEWS, P. C., PROCTOR, M. R. E., RUCKLIDGE, A. M. & WEISS, N. O. 1993 Pulsating waves in nonlinear magnetoconvection. *Phys. Lett.* A. **183**, 69–75.

MATTHEWS, P. C., PROCTOR, M. R. E., RUCKLIDGE, A. M. & WEISS, N. O. 1994 Nonlinear three-dimensional magnetoconvection in a compressible atmosphere. In *Solar Magnetic Fields* (ed. M. Schüssler & W. Schmidt), pp. 279–281. Cambridge University Press.

MATTHEWS, P. C. & RUCKLIDGE, A. M. 1993 Travelling and standing waves in magnetoconvection. *Proc. R. Soc. Lond.* A **441**, 649–658.

MOORE, D. R. & WEISS, N. O. 1990 Dynamics of double convection. *Phil. Trans. R. Soc. Lond.* A **332**, 121–134.

PROCTOR, M. R. E. 1992 Magnetoconvection. In *Sunspots: Theory and Observations* (ed. J. H. Thomas & N. O. Weiss), pp. 221–241. Kluwer, Dordrecht.

PROCTOR, M. R. E. & WEISS, N. O. 1982 Magnetoconvection. *Rep. Prog. Phys.* **45**, 1317–1379.

PROCTOR, M. R. E.& WEISS, N. O. 1993 Symmetries of time-dependent magnetoconvection. *Geophys. Astrophys. Fluid Dyn.* **70**, 137–160.

PROCTOR, M. R. E., WEISS, N. O., BROWNJOHN, D. P. & HURLBURT, N. E. 1994 Nonlinear compressible magnetoconvection. Part 2. Streaming instabilities in two dimensions. *J. Fluid Mech.* **280**, 227–253.

RUCKLIDGE, A. M. & MATTHEWS, P. C. 1993 Shearing instabilities in magnetoconvection. In *Theory of Solar and Planetary Dynamos* (ed. M. R. E. Proctor, P. C. Matthews & A. M. Rucklidge), pp. 257–264. Cambridge University Press.

RUCKLIDGE, A. M. & MATTHEWS, P. C. 1995 Analysis of the shearing instability in nonlinear convection and magnetoconvection. *Nonlinearity*, submitted.

RUCKLIDGE, A. M., SCHMIDT, H. U. & WEISS, N. O. 1995 The abrupt development of penumbrae in sunspots. *Mon. Not. R. Astron. Soc.* **273**, 491–498.

RUCKLIDGE, A. M., WEISS, N. O, BROWNJOHN, D. P. & PROCTOR, M. R. E. 1993 Oscillations and secondary bifurcations in nonlinear magnetoconvection. *Geophys. Astrophys. Fluid Dyn.* **68**, 133–150.

THOMAS, J. H. & WEISS, N. O. 1992 The theory of sunspots. In *Sunspots: Theory and Observations* (ed. J. H. Thomas & N. O. Weiss), pp. 3–59. Kluwer, Dordrecht.

WEISS, N. O. 1991 Magnetoconvection. *Geophys. Astrophys. Fluid Dyn.* **62**, 229–247.

WEISS, N. O., BROWNJOHN, D. P., HURLBURT N. E. & PROCTOR, M. R. E. 1990 Oscillatory convection in sunspot umbrae. *Mon. Not. R. Astron. Soc.* **245**, 434–452.